A Study of The Structural, Optical and Electrical Properties of Pristine Batio$_3$ Ceramic Material

ARPITA PATEL[1], RAJESH KUMAR KATARE[2]
[1, 2] *Department of Physics, SAGE University, Indore, India*

Abstract*—This paper discusses the preparation and experimentation of $BaTiO_3$ ceramic material. The solid state reaction method was used to prepare the sample. The desired crystal structure, formation of phase, and acquired lattice structure of the as synthesized sample was confirmed by X-ray diffraction technique and verified by a reliable method known as Rietveld refinement. The electrical properties viz dielectric loss and permittivity of the aforementioned compound were investigated in more detail. The synthesized sample has a tetragonal crystal structure and exhibits the P4mm space group, as revealed from the analysis of the XRD data. The absence of any new impurity phase within the bounds of experimentation is evident from the non-existence of additional reflection peaks in the XRD spectrum and its noise free nature. This indicates that the sample is a single phased material. The sample shows considerable dielectric properties which includes higher permittivity and lower loss tangent values as a function of the applied field, as revealed by the dielectric studies. Additionally, ac conductivity studies displays insulating nature of the sample. Impedance investigations were conducted in order to highlight the conduction mechanism. The research showed that the sample inherits a non-Debye character, that time constants are distributed, and that a single semicircle infers the role of grain boundaries in the conduction mechanism.

***Index Terms*- $BaTiO_3$, Ferroelectric materials; X-ray diffraction, dielectric nature; impedance spectroscopy; energy bandgap.**

I. INTRODUCTION

For electromechanical device applications, the most popular piezo-ceramic material is lead zirconate-titanate [Pb(Zr,Ti)O_3 (PZT)] [1]. As lead is known to be harmful and have negative effects on the environment, during the past 50 years, a great deal of research has been done on lead-free piezoelectrics. Alkaline-niobate-based lead-free piezoelectrics with characteristics similar to PZT were described by Saito et. al. [2]. Temendous research and literature is available on the studies of lead-free piezo-electrics since the publication of this study. The rapidly growing scientific community swiftly went back to the groundbreaking research on alkaline-bismuth-titanate-based piezoelectrics published by Takenaka et al. in 1991[3]. Research efforts thereafter concentrated on methods to enhance these materials' piezoelectric qualities. These tactics have included texturing, microstructure optimization, and looking for systems with polymorphic or morpho-tropic phase boundaries [4].

It is actually the exceptional dielectric qualities that makes $BaTiO_3$ the most significant electro-ceramic materials and is widely utilized in MLCC's [5]. Modern electrical systems, such electric cars and data transit and storage devices, are driving up the market for additional high-performance dielectrics. This implies that in addition to a high capacitive volumetric efficiency, future capacitor designs will require greater voltage operations at higher temperatures. By suppressing voltage saturation, it is possible to achieve lower non-linear permittivity. When combined with increased degradation resistance, this would be a significant technical improvement for these crucial materials [4-6].

Due to its superior dielectric qualities, barium titanate with a perovskite structure has garnered a lot of interest in lead-free devices such electro-optical, multilayer capacitors, thermistors and electromechanical devices. To our understanding, BaTiO3 is a potential catalyst, but there haven't been many publications on it. This could be because of the photo-catalyst's inherent disadvantages, such as its high band gap (3.18 eV). Furthermore, a high rate of charge recombination may lessen the intrinsic efficacy as a photo-catalyst for $BaTiO_3$ [7,8].

As $BaTiO_3$ inherits exceptional multifunctional properties, it is hot spot in the materials research field for last 7 decades. First of all, it is incredibly stable both physically and chemically. Secondly, it has

ferroelectric characteristics both above and below room temperature. Lastly, it is simple to make and use in the form of ceramic polycrystalline samples. Barium titanate has been utilized in capacitors and MLCs because its permittivity values are quite large accompanied loer loss tangent features. One of the most significant ferroelectric ceramics is doped barium titanate, which finds extensive use in piezoelectric devices, semiconductors, and PTC thermistors. Barium titanate belongs to a broad class of substances known as the perovskite family. Perovskite-structured ceramics are integrated and indispensable members of the electronic materials [9,10].

II. REVIEW OF LITERATURE

The $BaTiO_3$ sample structures synthesized by solid-state route at maximum sintering temperatures of 1350, 1400, 1410, and 1500°C were studied by Busha et al. The XRD data analysis displayed in Figure 1 demonstrates that the samples contain the cubic $BaTiO_3$ phase with an effective content of roughly 30% in addition to the tetragonal phase. On the surface of tetragonal-shaped ceramic grains, the cubic phase was seen as a thin coating [11].

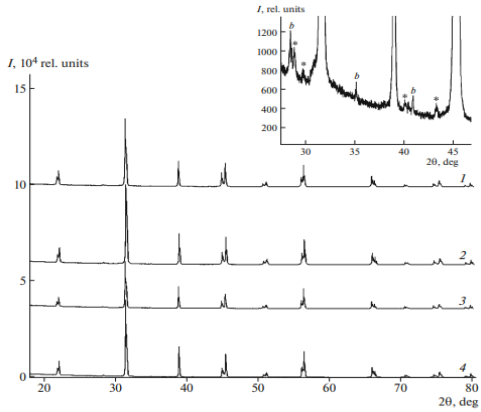

Figure 1: XRD diffraction patterns of barium titanate–nickel composites (BaTiO3–Ni)

Phong et. al. examined the optical, electrical conductivity, and structural characteristics of hydrothermally produced $BaTi_{1-x}Co_xO_3$ ($0 \leq x \leq 0.1$) ceramics. The study of the X-ray diffraction data shown in Figure 2 shows that the prepared samples have a P4mm symmetric single-phase tetragonal structure. Figure 3 displays UV-vis diffuse reflectance spectrum which demonstrates how Co concentration affects the direct optical band gap of $BaTi_{1-x}Co_xO_3$ ceramics. As the concentration of Co rises from 0 to 0.1, the optical band gap moves from 3.14 eV to 3.44 eV [12].

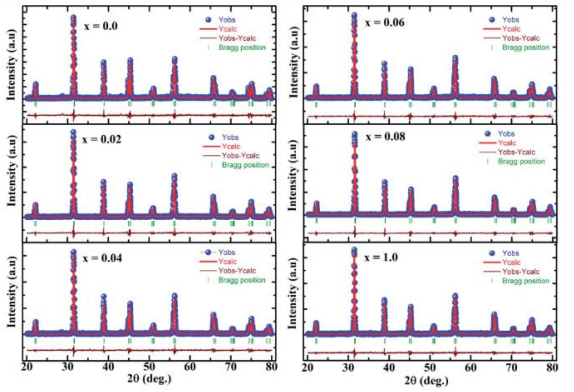

Figure 2: Rietveld Refinement of XRD data of $BaTi_{1-x}Co_xO_3$ ($0 \leq x \leq 0.1$) samples

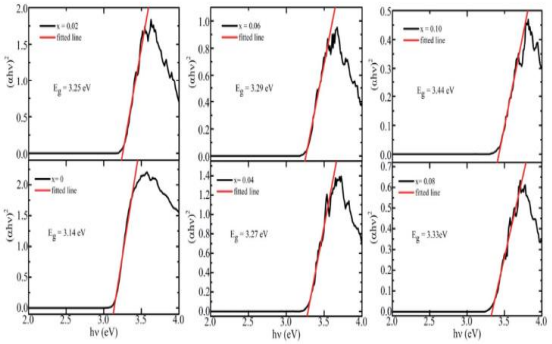

Figure 3: Optical band gap estimation of $BaTi_{1-x}Co_xO_3$ ($0 \leq x \leq 0.1$) samples

Lee et al. a1. reported on thin films of $BaTiO_3$ prepared by sol-gel spin-on processing developed on (111)Pt/Ti/SiO_2/Si substrates. The ac conduction mechanism and dielectric properties viz permittivity and dissipation of the material were addressed in response to temperature, frequency, and amplitude of the *ac* oscillation. Figure 4 shows that the dielectric constant and dielectric loss at 100 kHz are exceptionally better. Additionally, well above critical temperature,Tc, and frequency below the value of 100 Hz thin films of $BaTiO_3$ displayed a noticeable relaxation [13].

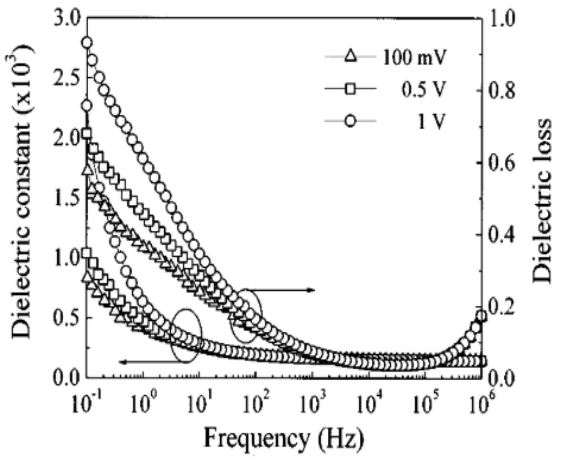

Figure 4: Dielectric characteristics of $BaTi_{1-x}Co_xO_3$ ($0 \leq x \leq 0.1$) samples

Hariom et al. [14] established a connection between the calcination temperature and the dielectric characteristics of $BaTiO_3$ nano-particles synthesized by the sol-gel method. The structural, morphological, elemental, chemical, dielectric and gas sensing properties have all been characterized using various techniques. At different temperatures, frequency-dependent dielectric characteristics were examined, as shown in Figure 5

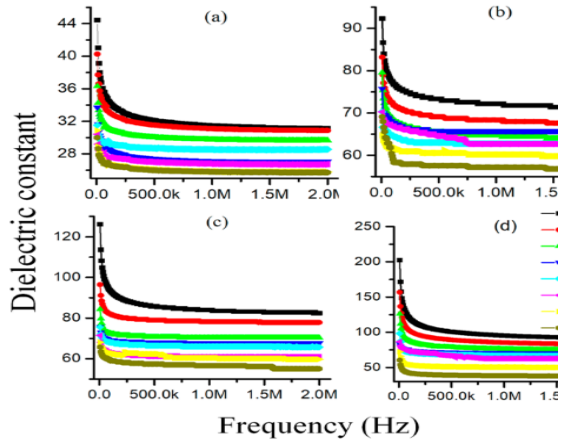

Figure 5: Dielectric characteristics of $BaTiO_3$ nanoparticles

Chena et al. [15] reports impedance analysis on $BaTiO_3$ (BT) particles represented as 0.25 $Bi(Zn_{1/2}Ti_{1/2})O_3$–$0.75BaTiO_3$ systems. The impedance data of BT, 0.25BZT-0.75BT, and BT@x(0.25BZT-0.75BT) (x=0.5–1.0) ceramics is shown as Figure 6. The data was collected, plotted and fitted using various equivalent circuits.

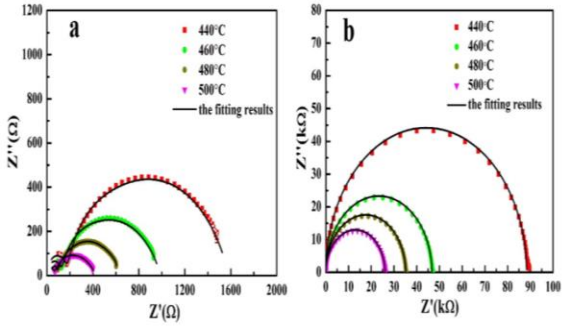

Figure 6 Impedance data fitting of data BT (a), 0.25BZT-0.75BT (b)

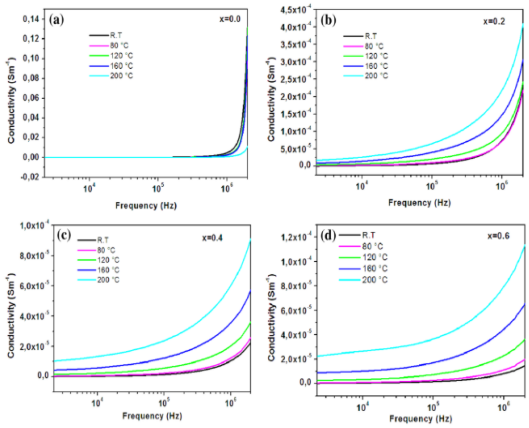

Figure 7: ac conductivity of ($BaTi_{1-x}Fe_xO_3$) with x = 0.0, 0.2, 0.4 and 0.6

Gouita et. al. examined Fe^{3+} doped $BaTiO_3$ ($BaTi_{1-x}Fe_xO_3$), prepared via the solid-state reaction method, sintered for six hours at 1200 °C, and calcined at 1100 °C with x = 0.0, 0.2, 0.4, and 0.6 Fe^{3+} concentrations. Tetragonal structure for $BaTiO_3$ at x=0.2 was discovered by the X-ray diffraction patterns spectrum. The hexagonal phase has been witnessed for Fe concentrations of 0.4 and 0.6. A decrease in grain resistivity of boundaries, a positive temperature coefficient of resistivity behavior for pure BT, and a negative temperature coefficient of resistivity behavior for the BTF materials were all inferred from studies of the complex electrical impedance and electrical modulus plots. It is discovered that the test materials' relaxing behavior is not of the Debye type. The ac conductivity of ($BaTi_{1-x}Fe_xO_3$) with x = 0.0,0.2,0.4 and 0.6 ceramics is studied and demonstrated as Figure 7 [16].

$BaTiO_3$ nanoparticles made using the sol-gel process and spanning four distinct size ranges were shown by Ramakanth et. al. These ferroelectric nanoparticles have a significant increase in optical absorption arising from lowered optical band gap values, which at various size ranges are down from 3.2 eV to 2.53 eV as displayed as Figure 8. These intriguing feature reveal them to be potential candidates for light energy harvesting. Exchange correlation interactions between the carriers in the particles, which have a decreased band gap of 3 eV and 2.53 eV, are responsible for the improved optical absorption in the 23 nm and 54 nm size particles. The absorption bleached in particles in the 31 nm and 34 nm range, showing larger band gaps of 3.08 eV and 3.2 eV, respectively [17].

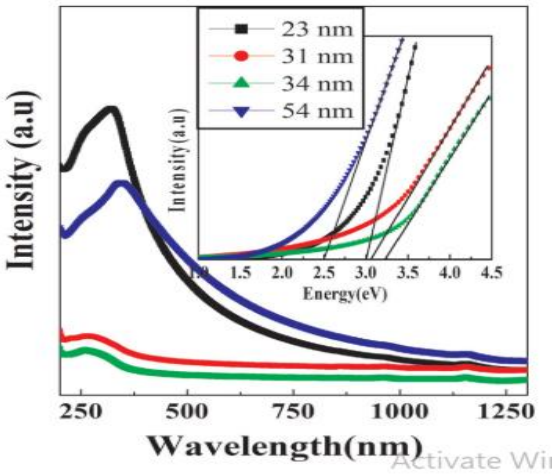

Figure 8: Tuac's plot of $BaTiO_3$ with different nano-sizes

III. EXPERIMENTAL DETAILS

3.1 Synthesis

High temperature solid state technique [18] was used to prepare polycrystalline $BaTiO_3$. Using acetone to ensure adequate dispersion, the stoichiometric amounts of the starting ingredients, titanium dioxide (TiO_2) and barium carbonate ($BaCO_3$), were combined for five hours in an agate mortar. For five hours, the mixture was calcined at 1000 ^oC. After being calcined further for three hours, the material was once more crushed to a fine powder and heated to 1100 ^oC for five hours. Applying a pressure of 5 tons per inch, the double-calcined sample was transformed into the pellets and these pellets were sintered for 7 hours at 1200 degrees Celsius. To obtain smooth electrical connections for dielectric and other electrical measurements, the compact disc-shaped pellets underwent a final process of silvering.

3.2 Experimentation

To establish the acquired crystal structure and formation of phase by the synthesized $BaTiO_3$ sample, we employed X-ray diffraction (XRD) characterization technique. A PROTO AXRD Benchtop Diffractometer using Cu-Kα1 radiation (λ = 1.5406 Å) was used for the experiment. The samples were put through dielectric tests using Precision LCR meter, Model E4980A from Keysight Technologies. The measurement lies in frequency range of 2Hz-2MHz.

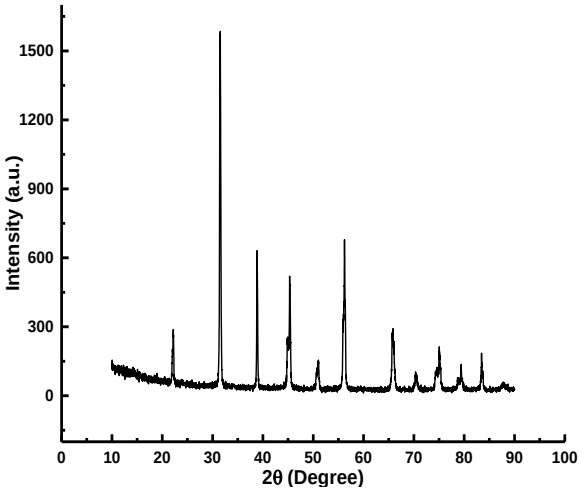

Figure 9: X-ray diffractogram of $BaTiO_3$ compound

IV. RESULTS AND DISCUSSIONS

4.1 X-ray Diffraction (XRD) Data Analysis

X-ray Diffraction (XRD) patterns of the polycrystalline $BaTiO_3$ sample is displayed as Figure 9. The study of the XRD diffractogram was revealed tetragonal structure for synthesized sample with assigned space group P4mm. There are no further reflection peaks seen in the sample's X-ray diffractogram within the experiment's parameters. The sample is highly crystalline as evidenced by the high intensity and sharpness of the typical diffraction peaks, and their narrow full width at half maximum (FWHM) suggests a large mean crystallite size. Applying Scherer's equation, $t = k\lambda/(\beta \cos \theta)$, which takes into account the following: λ is the used X-ray

wavelength, t is the particle's diameter, K is a geometrical form factor, commonly taken to be 0.9, θ is the Bragg's diffraction angle, and β is FWHM of some characteristic diffraction peaks, yielded the average size of the crystallites. The mean size of crystallites on average was estimated to be 90 nm.

Figure 10: Rietveld refinement of X-ray diffraction

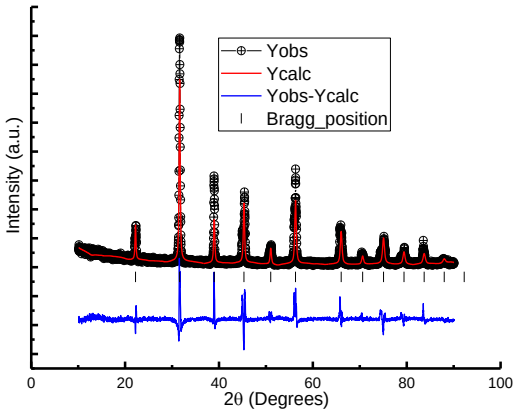

data of $BaTiO_3$ compound

Table 1: Rietveld refinement results of $BaTiO_3$	
Crystal structure	Tetragonal
Space group	P4mm
Axial angle relation	$\alpha=\beta=\gamma=90^o$
Lattice arameters (Å)	$a=b$=3.9271, c=3.9982
Volume ($Å^3$)	63.0819
Density(g/cm^3)	3.6829
GoF	2.2
χ^2	3.23

To verify the results and revelations obtained from analysis of XRD spectrum, we used FullProf Software. Figure 10 displays the refinement of the XRD data. The refinement of the XRD data various calculates structural parameters demonstrated as Table 1 and thereby reveals the crystallization of the sample, confirms phase formation and establishes the space group acquired by the sample.

4.2 Dielectric Studies

The electric permittivity (ε') of the $BaTiO_3$ sample as prepared is depicted in Figure 11 as a response to frequency. It is clear that at elevated frequencies, ε' attains a field independent value and then drops with frequency. At the interface, the charge accumulation is reduces because the ac field reverses more frequently at higher frequencies. The ion diffusion mechanism explains the constant value of ε'. The ionic medium becomes net polarized at frequencies of the lowervalues when charges build up at the interface area. The ε' rises as a space charge region forms at the electrode-electrolyte interface [15, 19].

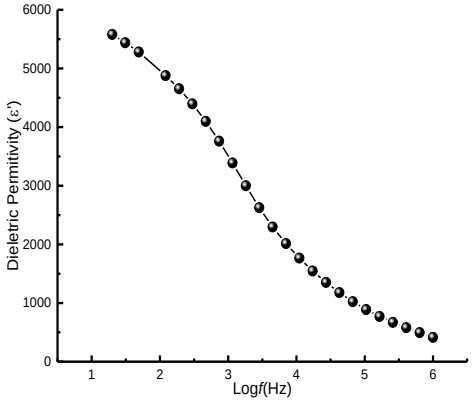

Figure 11: Dielectric Permitivity(έ) of $BaTiO_3$

The frequent polarization that occurs in the $BaTiO_3$ sample is the cause of the drop in the ε' in the lower frequency band. The electric dipoles lag behind the applied external field because they do not follow it. The Maxwell-Wagner model, which states that a dielectric material is composed of good conducting grains divided by low conducting grain boundaries, can explain the higher dielectric constant values of the as prepared samples at frequencies in the lower region of the applied field and lesser έ at higher frequencies. Polarization falls and hence the έ falls when the probability of electrons reaching the grain boundary increases in an ac field because of their reverse motion.

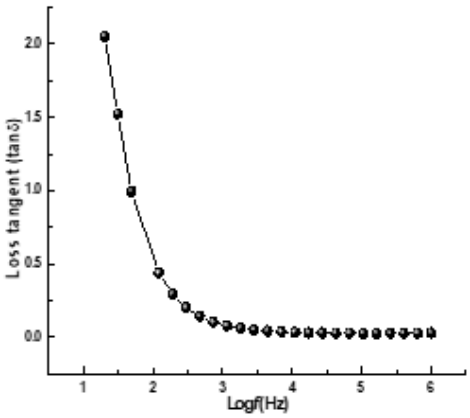

Figure 12: Dielectric permittivity (Ɛ″, imaginary) of $BaTiO_3$ compound

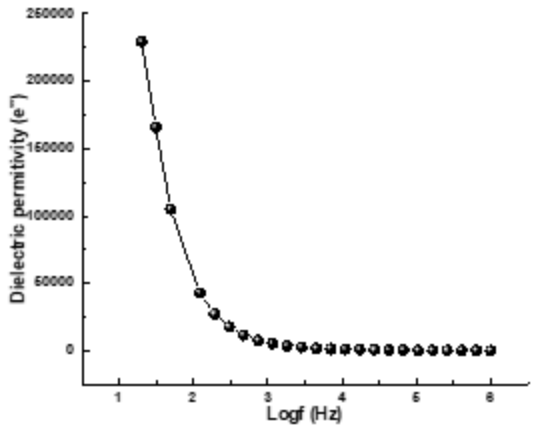

Figure 13: Dielectric loss tangent (tanδ) as a function of frequency of $BaTiO_3$

The field independent έ for elevated frequency values reveals that applied field and charge hopping between different sites are not in agreement i.e. ion hopping doesn't abbey applied ac field values as a result the independent behaviour is observed [19,20].

Figure 12 illustrates how ε″ decreases as frequency increases. Three different effects can be considered to contribute to the size of ε″: dc conductance, interfacial polarization, and the typical dipole orientation, also known as Debye loss [21]. The interfacial polarization could be the reason for this reduction in ε″ with increasing frequency. Once more, there was no peak seen in the measured frequency range for the ε″–f plots. Interfacial polarization is typically obscured by conduction because disordered systems have conductive parts [22].

The dielectric dissipation/ loss relying on frequency of the $BaTiO_3$ perovskite sample is displayed in Figure 13. At frequencies in the lower region of applied field, the loss tangent displays a decreasing trend from its higher value with enhanced frequency of the field. The behavior is comparable to that of the frequency-dependent έ. The phenomenological model proposed by Koop et. al explains well the observed reduction in the dielectric loss tangent with rise in frequency. When polarization is unable to obey the applied ac field, dielectric loss is caused by impurities and structural inhomogeneities [23-25].

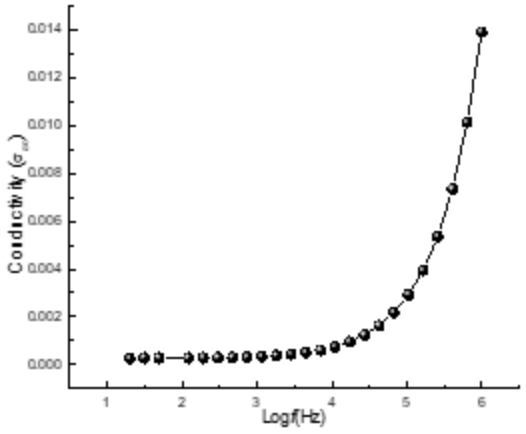

Figure 14: ac conductivity of $BaTiO_3$ compound

The *ac* conductivity of $BaTiO_3$ compound is shown in Figure 14. Up to a certain field value, the *ac* conductivity is nearly irresponsive to the applied field; beyond that, the conductivity increases sharply as the applied field increases. The ordered motion of charge carriers caused by an applied field is what causes electrical conduction, and this process is thermally stimulated. It relies strictly on the properties of charge carriers and how they react to the given circumstances.

Under the impact of applied, the hopping of charge carriers between adjacent lattice sites, aiding in the conduction mechanism. The release of charge carriers from defects and trap centers is responsible for the sudden increase in ac conductivity that occurs beyond a particular field value [12,26].

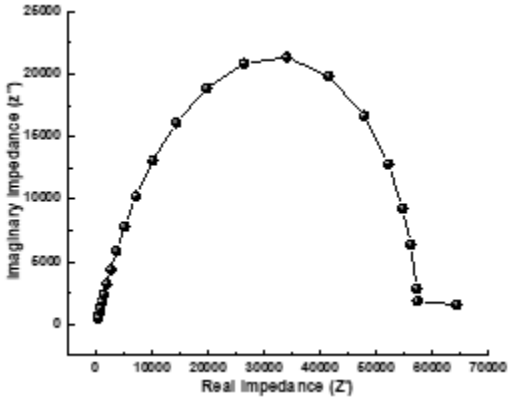

Figure 15: Nyquist's plot of $BaTiO_3$ dielectric compound

4.3 Impedance Studies

The complex impedance (CIS) characterization examines how the systems react to periodic small-amplitude signals, which provide details about the structure, interactions, and interface itself. Effective CIS research identified several pathways involved in both the relaxation and conduction processes. At zero bias voltage, we recorded the complex impedance spectra of the material under observation which is illustrated in Figure 15.

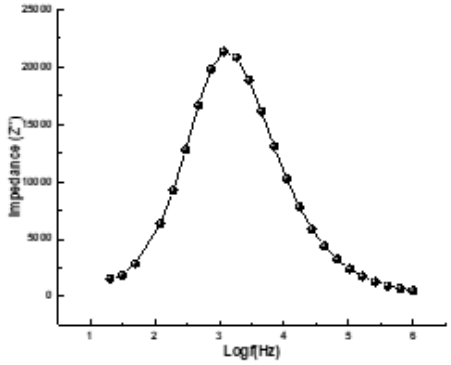

Figure 16: Impedance (Z') of $BaTiO_3$ dielectric compound

When there is only one semicircle visible, the sample's grain characteristics are the source of the resistance. The total grain resistance is found at the low frequency side semicircle intersection. A depressed semicircle arc with a center that is far from the origin is shown in the plot, which is suggestive of the sample's non-Debye character. Also, the higher diameter of the semicircle reveals the higher resistive material [27,28].

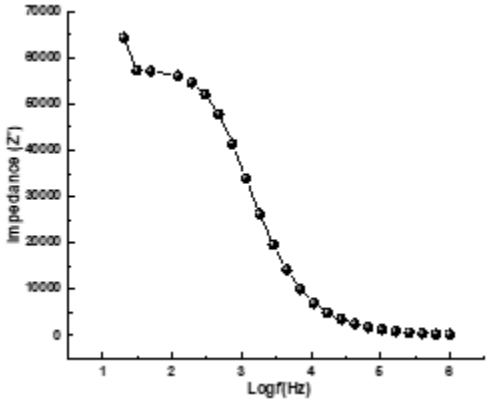

Figure 17: Impedance (Z'') of $BaTiO_3$ dielectric compound

The frequency depending nature of impedance (Z ') is displayed in Figure 16. The real part of impedance monotonically decreases as frequency rises (over 10 kHz), and a constant value—that is, frequency independence—is noted. The merging trend at elevated frequency values may be attribute of release of space charge or a lowering tendency in barrier characteristics [28,29]. Figure 17 inset displays the imaginary component of impedance (Z″), which is depending on frequency. The ZCC variation shows the distribution of relaxation time. The oxygen ion vacancies hopping in a particular location is expected to be the reson behind the electrical conductivity [30–32].

ACKNOWLEDGEMENTS

Authors acknowledge the SAGE University as an institute and department of physics sage university and its faculty for constant support. GHS College, Indore (M.P.), department of Physics, Dr. Netram Kaurav (Materials Research Lab, GHS College, Indore (M.P.) are extended warm thanks for extending support

REFERENCES

[1] M. M. Mikhailov, V. Y. Ul'yanitskii, A. A. Lovitskii, *et al. . Russ Phys J*, 60 (2017).1077–1079

[2] Y. Saito *et. al. Appl. Phys. Express* 15 (2022) 021002

[3] T. Takenaka, K. I. Maruyama and K. Sakata, Jpn. J. Appl. Phys., 30 (1991) 2236-2239.

[4] M. Acosta, N. Novak; V. Rojas *Appl. Phys. Rev.* 4, 041305 (2017)

[5] D. Masekela et. al. Arabian Journal of Chemistry, 16 (2023) 104473

[6] M. Fakhar-e-Alam, S. Saddique, N. Hossain, *et. al. J Clust Sci* 34, 1745–1755 (2023)

[7] K. Suzuki and K. Kijima *Jpn. J. Appl. Phys.* 44 (2005) 2081

[8] S. Ramakanth; K. C. James Raju, Journal of Applied Physics 115(2014):173507

[9] V. Sydorchuk et. al. Physicochem. Probl. Miner. Process., 58(2) (2022) 147192

[10] V. Buscaglia et. al. Encyclopedia of Materials: Technical Ceramics and Glasses 3 (2021) 311-

344

[11] A. A. Busha, V. P. Sirotinkinb, and S. A. Ivanov, Crystallography Reports, 65 (2020) 1025–1032

[12] L. T. H. Phong, N. T. Dang, N. V. Dang, RSC Adv., 2022, 12, 16119

[13] S. J. Lee, K. Y. Kang, and S. K. Han, Appl. Phys. Lett., 75 (1999)

[14] H. Pawar, M. Khan, M. Kumari1, Applied Physics A 127 (2021) 384

[15] W. Chena , H. Haoa, Y. Yang et. al. Ceramics International 43 (2017) 8449–8458

[16] N. Gouita, T. Lamcharfi, M. Bouayad et. al. Journal of Materials Science: Materials in Electronics https://doi.org/10.1007/s10854-018-8666-3

[17] S. Ramakanth1 and K. C. James Raju, Journal of Applied Physics 115, 173507 (2014)

[18] M. T. Buscaglia, M. Bassoli, V. Buscaglia, J. Am. Ceram. Soc. 88 (2005) 2374–2379.

[19] X. Wu, H. Zhao,W. Han et. al. *RSC Adv.*, 13 (2023) 11002-11009

[20] G. Arlt, D. Hennings, G. de With, *J. Appl. Phys.* 58, 1 (1985) 619–1625

[21] F.I.H., Rhouma,, A. Dhahri, J. Dhahri, *et al. Appl. Phys. A* 108 (2012) 593–600

[22] Y. Xi, Y. Bin, C. K. Chiang and M. Matsuo Carbon 45 (2007) 1302

[23] D. Hennings, Int. J. High Technol. Ceram. 3 (1987) 91–111.

[24] D. F. K. Hennings, B. S. Schrenemacher, H. Schrenemacher, J. Am. Ceram. Soc. 84 (2001) 2777–2782

[25] M. Boulos, S. G. Fritsch, F. Mathieu, B. Durand, T. Lebey, V. Bley, Solid State Ion. 176 (2005) 1301–1309.

[26] B. Ertuğ, Sensors and Materials, 25 (2013) 309–321.

[27] W. Chen, H. Hao, Y. Yang, Ceram. , 43 (2017) 8449-8458

[28] N. Hirose, A.R. West, J. Am. Ceram. Soc. 79 (1996) 1633–1641.

[29] Y. Sun, H.X. Liu, H. Hao, L. Zhang, et al., Ceram. Int. 41 (2015) 931–939.

[30] A. Eršte, et al., Adv. Appl. Electroceram. II (2012) 23–29.

[31] J. C. C. Abrantes, J. A. Labrincha, J. R. Frade, Mater. Res. Bull. 35 (2000) 727–740.

[32] J. C. C. Abrantes, A. Feighery, et al., J. Am. Ceram. Soc. 85 (2002) 2745–2752